

Adhesion of Osteoblasts to a Vertically Aligned TiO₂ Nanotube Surface

Ekaterina Gongadze^{1,2}, Doron Kabaso¹, Sebastian Bauer³, Jung Park⁴, Patrik Schmuki³ and Aleš Igljč^{1,2,*}

¹Faculty of Electrical Engineering, University of Ljubljana, Tržaška 25, SI-1000 Ljubljana, Slovenia; ²Department of Orthopedic Surgery, Faculty of Medicine, University of Ljubljana, Zaloška 9, SI-1000 Ljubljana, Slovenia; ³Department of Materials Science, Friedrich-Alexander-University of Erlangen-Nuremberg, Martensstr. 7, D-91058 Erlangen, Germany; ⁴Department of Pediatrics, Division of Molecular Pediatrics, University Hospital, Erlangen, Erlangen, Germany

Abstract: The adhesion of cells to vertically aligned TiO₂ nanotubes is reviewed. The attraction between a negatively charged nanotube surface and a negatively charged osteoblast is facilitated by charged protein-mediators like proteins with a quadrupolar internal charge distribution, fibronectin and vitronectin. It is shown that adhesion and spreading of osteoblasts on vertically aligned TiO₂ nanotube surfaces depend on the diameter of the nanotubes. Apparently, a small diameter nanotube surface has on average more sharp convex edges per unit area than a large one, leading to stronger binding affinity on its surface.

Keywords: TiO₂ nanotube surfaces, adhesion, dynamic simulations, nanostructured surface topography, osteoblast adhesion.

INTRODUCTION

Orthopaedic implants are of immense importance at the end stage of destructive joint diseases like osteoporosis and osteoarthritis. Demand for implants is continuing to rise sharply due to constant growth in the elderly population worldwide. To address this challenge, modelling and simulation of the interactions between the implant and the surrounding body tissue have become of increasing importance. This mini-review is focused on the interactions of osteoblasts with nanostructured titanium surfaces.

It was observed recently that roughness of titanium surfaces alone influences the adhesion of osteoblasts and their spreading and proliferation. In the past, the influence of the roughness of the titanium surface on osteoblast attachment was studied mainly at micrometre scale [1-6], while in recent times more attention was paid to the nanostructured titanium surface as a vertically aligned TiO₂ nanotube surface [6-8]. In order to elucidate the behavior of osteoblasts in response to the nanostructured surface topographical effect, in this mini-review the possible mechanisms of adhesion of cells to a vertically aligned TiO₂ nanotube surface (Fig. 1) are discussed.

FORMATION OF TiO₂ NANOTUBE SURFACE

Smooth surfaced titanium sheets (99.6 percent purity, Advent Ltd.) may be used as substrates for the anodic growth of TiO₂ nanotube layers [7,9]. Before electrochemical anodization all samples should be polished to obtain smooth

surfaces. Thus the titanium sheets were mechanically ground, lapped and finally polished (New Lam System). For anodization an electrochemical cell with a three-electrode configuration was used. Platinum gauze served as the counter electrode and a Haber-Luggin capillary with an Ag/AgCl (1M KCl) electrode was used as the reference electrode. For electrochemical experiments a high-voltage potentiostat (Jaisle IMP 88-200 PC) was used. Electrochemical treatments were carried out in 1 M NaH₂PO₄ with addition of 0.12M HF [7, 9]. For nanotube formation, potentials of 1 V and 20 V at room temperature were applied for 2 hours and resulted in nanotube diameters of 15 nm and 100 nm, respectively, as shown in (Fig. 2) [7,9]. All electrolytes were prepared from reagent grade chemicals and deionized water. After electrochemical treatment, the samples were immersed in deionized water for two days to reduce the content of residual fluorides in the oxide structures produced, as shown in [9]. All samples were sterilized using an autoclave at 121°C prior to cell seeding. High resolution XRD of the nanotube layers after autoclaving showed the tubes to be amorphous in nature as shown [9].

THE MECHANISM OF OSTEOBLAST ADHESION TO THE TiO₂ NANOTUBE SURFACE

It was recently suggested that contact between the membrane of the osteoblasts and the titanium implant surface is established in two steps. Firstly, the osteoblast cell membrane makes non-specific contact due to electrostatic forces [5,6], followed by a second step where specific binding involving an integrin assembly in focal contact takes place [7,10,11]. A possible mechanism of osteoblast adhesion to the implant surface was proposed based on the assumption that positively charged proteins [6,12,13] or proteins with

*Address correspondence to this author at the Laboratory of Biophysics, Faculty of Electrical Engineering, University of Ljubljana, Tržaška 25, SI-1000 Ljubljana, Slovenia; Tel: +386 31 356 953; Fax: +386 1 476 88 50; E-mail: ales.igljc@fe.uni-lj.si

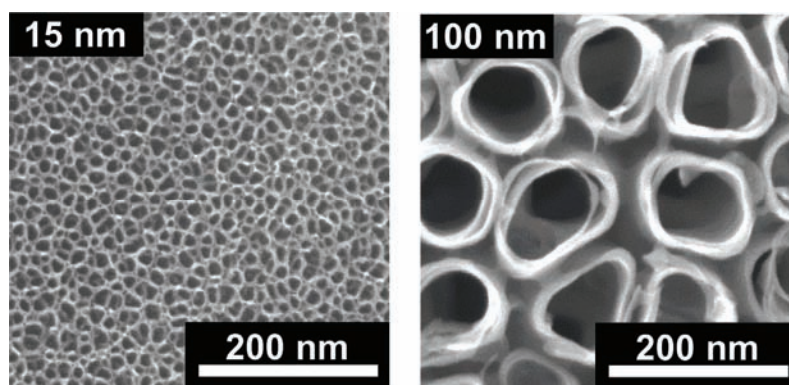


Fig. (1). Electron microscope images of the surface of layers of vertically self-aligned TiO₂ nanotubes. Note that the small diameter (15 nm) TiO₂ nanotubes are much more closely packed than the large diameter (100 nm) ones. The inner and outer diameter of a small diameter nanotube are approximately 10 and 15 nm, and the respective dimensions of a large diameter nanotube are approximately 80 nm and 100 nm. A field emission scanning electron microscope (FE-SEM, S-4800, Hitachi) was used.

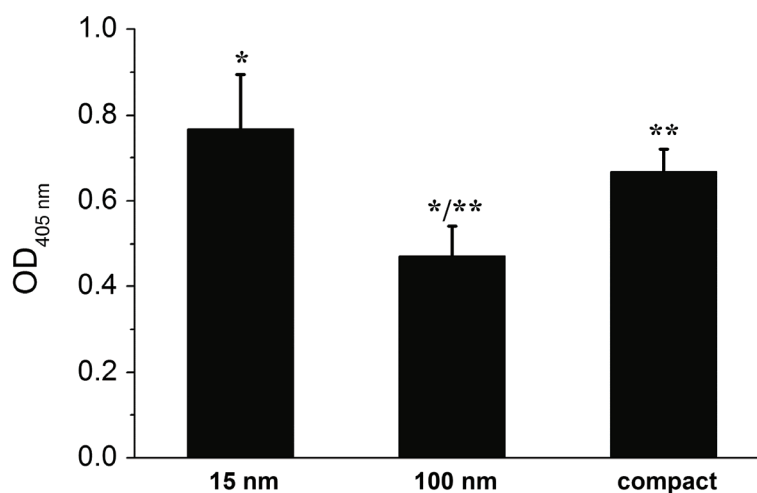


Fig. (2). Quantitative assessment of the amount of fibronectin adsorbed after two washing steps. On 15 nm diameter nanotubes significantly higher amounts of fibronectin was found adsorbed compared to 100 nm diameters (* $p = 0.0068$) as well as on compact surfaces compared to 100 nm nanotubes (** $p = 0.0042$). No statistical difference was found in between 15 nm nanotubes and compact (flat) surfaces ($p = 0.2014$).

positively charged tips, i.e. a quadrupolar internal charge distribution [5, 6] attached to the negatively charged implant surface, serve as a substrate for the subsequent attachment of negatively charged osteoblasts. It was shown [5] that for high enough negative values of the charge density of the titanium surface, proteins with positively charged tips are concentrated close to the charged surface and oriented in a direction perpendicular to it.

It was also shown [5] that a high surface charge density on the titanium surface and a high effective quadrupole moment of the protein (i.e. a distinctive internal quadrupolar charge distribution) can turn the repulsive force between a negatively charged titanium surface and the osteoblast surfaces into an attractive force. The corresponding attractive force is also called the bridging force [5,6,14]. The origin of attractive interactions between two negatively charged surfaces lies in the electrostatic attraction between the positively charged domains on the tips of the titanium surface-bound proteins with quadrupolar charge distribution and the negative charges of the opposite osteoblast membrane [5,6,14]. A

non-zero effective internal quadrupolar charge distribution does not exclude the presence of other charged protein groups (usually in pairs of positive and negatively charged groups) between the two positively charged protein tips [5, 6,14]. A typical example of a such bridging protein with positively charged tips is β_2 -GPI protein which may induce strong attraction between negatively charged surfaces [14,15]. In line with the predicted increased strength of the protein-mediated attractive bridging interaction between a titanium surface and an osteoblast with an increased surface charge density [5,6,14,15], we propose that the increased surface charge density at the sharp edges of a TiO₂ nanotube surface may promote protein-mediated adhesion of osteoblasts due to the increased accumulation of proteins with quadrupolar internal charge distribution, as well as the increased binding of fibronectin and vitronectin [6].

The origin of the increased binding of fibronectin at sharp edges of vertically oriented TiO₂ nanotube walls may be bridging and direct interaction forces [5,6,14,16,17]. Accordingly, it was indicated recently that an increase in the

negative net charge of a titanium surface promotes the fibronectin-mediated binding of osteogenic cell receptors [18]. In addition to fibronectin, human osteoblasts also adhere to vitronectin [1,19]. Like fibronectin, vitronectin too contains an Arg-Gly-Asp (RGD) sequence close to the somatomedin B domain which is responsible for integrin binding and cell adhesion [1,20]. The highly positively charged group of vitronectin near the C-terminal group on the other side of the vitronectin molecule is the binding site for negatively charged molecules of heparin [20-22]. It can therefore be anticipated that the highly positively charged heparin binding site of vitronectin may be predominantly (electrostatically) bound at the sharp and negatively charged convex edges of TiO₂ nanotubes. On the other hand, the vitronectin RGD binding site on the other side of the vitronectin molecule may bind to the integrin molecule, resulting in a facilitation of the osteoblast adhesion at sharp convex edges of TiO₂ nanotube walls.

To investigate any difference in fibronectin adsorption to surfaces structured with different diameters of TiO₂ nanotubes, the adsorption efficiency of fibronectin was measured quantitatively using ELISA immunoassay. Fibronectin (10 g/mL) was plated at a volume of 100 L on each sample (2×2 cm in size) and incubated overnight at 37°C. After washing twice with PBS, the samples were incubated with the antibody of rabbit polyclonal anti-fibronectin (Sigma) for one hour at room temperature. After washing away any unbound primary antibody with PBS twice for 5 minutes, the samples were further incubated with a 1:250 dilution of the biotinylated anti-rabbit secondary antibody (Jackson Immuno Research) for 30 minutes at room temperature. After washing with PBS two times for 5 minutes, the samples were further incubated with streptavidin-alkaline phosphatase complex for 30 minutes at room temperature. The samples were then incubated with alkaline phosphatase pNPP liquid substrate (Sigma) at 37°C for 4 hours, followed by washing with PBS twice for 5 minutes. Afterwards fibronectin adsorbed on the samples was quantitatively assessed with an ELISA plate reader at OD 405 nm.

In accordance with above suggested mechanism of osteoblast binding to TiO₂ nanotube surfaces, (Fig. 2) shows the quantitative ELISA results. These indicate strong differences in fibronectin adsorption to TiO₂ nanotube surfaces with different diameters. A significantly higher amount of fibronectin was found on 15 nm than on 100 nm nanotube diameters. No significant higher amounts of adsorbed fibronectin could be found on 15 nm diameters compared to compact (flat) surfaces. The increased fibronectin and vitronectin accumulation at the negatively charged edges of vertically oriented TiO₂ nanotubes can facilitate the clustering of integrin molecules, which enables the formation of focal adhesion complexes. Due to the larger density area of highly curved nanotube edges, the small diameter TiO₂ nanotube surface has a significant larger portion of fibronectin adsorbed and thus more integrin binding regions than the large diameter TiO₂ nanotube surface. Since there is no significant difference in the binding of fibronectin on the small diameter TiO₂ nanotube surface and a flat titanium surface (Fig. 2), one can conclude that the strength of the attractive interactions per unit area of the edges of TiO₂

nanotube is larger than the corresponding value for a flat titanium surface.

It should be stressed at this point that the semiconductor TiO₂ nanotube layer is much thicker than the very thin oxide layer formed on a flat titanium surface where the bulk titanium properties remain metallic. The surface of the semiconductor TiO₂ nanotubes has a certain number of surface titanium and oxygen dangling bonds, therefore OH⁻ and H⁺ ions and other ionic species present in the electrolyte can be chemisorbed /adsorbed to the TiO₂ nanotube surface in a curvature-dependent way. Also the ions present in the electrolyte used for fabrication the TiO₂ nanotubes can be chemisorbed or adsorbed on the TiO₂ nanotube surface. And finally, since the TiO₂ nanotubes are attached to the underlying metallic titanium foil, the conduction electrons are transferred from the titanium foil to the attached TiO₂ nanotubes. Within the classical approach, the solution side of the semiconductor (TiO₂) in contact with electrolyte solution is traditionally described using different mean-field electric double layer theories [23,24,] where the above described surface specific properties of TiO₂ may be captured in one phenomenological parameter, i.e. in the curvature-dependent effective surface charge density [6]. Therefore in the steady-state the non-zero TiO₂ nanotube curvature-dependent surface charge density is established at sharp edges of the TiO₂ nanotube wall, where the initial value of the surface Fermi energy is different from the other regions of the TiO₂ nanotube surface. Using the classical approach the accumulation of charge in the electrolyte at the TiO₂ surface can be described as a capacitor (described within the electric double layer theory) whose capacitance is curvature dependent. The condition of constant electric potential over the TiO₂ surface then implies a curvature-dependent surface charge density (see also [6]).

DYNAMIC MODEL OF OSTEOBLAST ADHESION TO THE TiO₂ NANOTUBE SURFACE

To shed light on the dynamics of membrane growth on the TiO₂ nanotube surface (Fig. 1) we constructed a computational model based on the membrane free energy of elasticity, which includes the binding energy of integrin molecules to the titanium surface and the nearest-neighbour attractive interaction energy between integrin molecules. The intrinsic shape of integrin molecules is taken into account in the spontaneous curvature in the expression for membrane bending energy. The model described below is an extension of previous theoretical models [6, 25-30].

The membrane shape explored in this model describes a segment of the osteoblast outer contour, where the membrane is initially flat. The membrane geometry is under the constraint of translational symmetry. Moreover, we assume that the membrane curvature along the direction perpendicular to the contour is roughly constant, and thus it enters our calculation as a modified membrane tension. The vertical intersection of small diameter and large diameter nanotube surfaces is modelled explicitly as a rectangular edge-like profile. For the case of small and large diameter nanotube surfaces, the widths of the repeating rectangular unit are 3 nm and 15 nm, respectively. According to the diameter of the nanotube surface, the corresponding

distances between the edges of consecutive rectangular units are 15 nm and 100 nm.

It is assumed that membrane regions adhering to the nanotube surface cannot be detached by the end of the simulation. This membrane trapping may be due to strong electrostatic interactions of the nanotube surface with the cell membrane and the binding of membrane integrin molecules to fibronectin at the nanotube surface. Regarding the integrin molecules in our model, we assume that their overall number in the membrane is conserved, and that they are allowed to move laterally along the osteoblast membrane. The maximal possible number of integrin molecules in the membrane segment is obtained from the total area divided by the cross-sectional area of the extracellular region of an integrin molecule. Our model investigates the coupling between the adhesion of osteoblast cells to the extracellular matrix, the interaction between integrin molecules, and their spontaneous curvature. The free energy expression is employed to derive the equations of motion of an osteoblast membrane contour and the integrin density distributions. The membrane free energy in our dynamic model is:

$$F = \int \left(\frac{1}{2} \kappa (H - \bar{H})^2 + \sigma_t + \varphi_s h^2 - \omega n_s n - n_s \frac{c\Omega}{2} n^2 + kT n_s n \right) dA, \quad (1)$$

where the first term gives the bending energy due to the mismatch between the membrane curvature and the membrane spontaneous curvature of integrin molecules, κ is the bending modulus, H is the local membrane mean curvature, \bar{H} is the intrinsic mean curvature due to embedded integrin molecules and n is the area fraction density of integrin (relative density). The second term σ_t is the Lagrange multiplier (having the units of membrane surface tension) for the conservation constraint of the total membrane area. The third term gives the energy due to the force of the cytoskeleton inside cells and φ_s is the restoring cytoskeleton spring constant. The fourth term is the negative binding potential of integrin molecules ($\omega > 0$). The fifth term describes the direct interaction Bragg-Williams term between neighboring integrin molecules. The sixth and seventh terms are the entropic energies, taking into account the finite areas of integrin molecules. Ω is the direct-interaction Bragg-Williams constant ($\Omega > 0$), c is the number of the nearest neighbour integrin molecules, $h = h(s)$ describes the magnitudes of small deformations from the flat membrane, and $n_s = 1/a_0$ is the saturation area density of integrin molecules, where a_0 is the cross-sectional area of a single integrin molecule.

It is assumed that the aggregation and binding of integrins can occur only at the top surface of the rectangular profile (i.e. above the edge regions of the nanotube surface). Therefore, the binding constant (ω) and the interaction constant (Ω) are positive only in membrane regions above the edges of the nanotube surface. In the following the free energy is normalized with respect to d_m so $F/d_m \rightarrow F$, and as

a result, the free energy is considered to vary along the membrane contour. The variation in the direction perpendicular to the membrane contour is assumed to be constant. We next derive the equations of motion of the membrane contour using differentiation of the free energy (Eq. (1)) with respect to the membrane coordinate [6,26,28] and integrin concentration. To take into account the drag due to viscous forces, we assume for simplicity only local friction forces with coefficient ξ . For the nearly flat osteoblast membrane, the equation of motion of the membrane is given by

$$\xi \frac{\partial h(s)}{\partial t} = - \frac{\delta f}{\delta h(s)} \quad (2)$$

where t is time, and f is F/dA . Note that the force density $\frac{\delta f}{\delta h(s)}$ equals the membrane shape velocity times the friction coefficient, but is opposite in direction. Since the relative change in the y (i.e. vertical, $y=h(s)$) direction is considerably greater than the change along the x (i.e. horizontal) direction, we only consider changes along the vertical y direction.

Differentiation of the free energy (Eq.(1)) is projected to give the forces normal to the membrane contour. We now list the forces derived from differentiation of the free energy (Eq. (1)):

$$F_{curvature} = \kappa \left(-\nabla^2 H + \bar{H} \nabla^2 n + \frac{1}{2} n^2 \bar{H}^2 H + \frac{1}{2} H^3 \right), \quad (3)$$

$$F_{tension} = \sigma_t H, \quad (4)$$

$$F_{binding} = -\omega n_s n H, \quad (5)$$

$$F_{spring} = -2\varphi_s h, \quad (6)$$

$$F_{entropy} = kT n_s [n \ln(n) + (1-n) \ln(1-n)] H, \quad (7)$$

$$F_{interaction} = -c\Omega n_s n^2 H / 2, \quad (8)$$

where $F_{curvature}$ is the force due to the curvature energy mismatch between the membrane curvature and the spontaneous curvature of the integrin molecules, $F_{tension}$ is the membrane tension force, $F_{binding}$ is the force due to binding of integrin molecules, F_{spring} is the spring restoring force, $F_{entropy}$ arises from the entropy of the integrin molecules in the membrane, which acts to expand the length of the contour, and $F_{interaction}$ is the force due to the direct interaction between neighboring integrin molecules. The non-linear term $0.5 H^3$ in $F_{curvature}$ in the following is neglected. We now calculate the dynamics of the integrin density, using the following conservation equation:

$$\frac{\partial n}{\partial t} = -\nabla \cdot \vec{J} = \frac{\Lambda}{n_s} \nabla (n \nabla \frac{\delta F}{\delta n}) - \frac{n}{ds} \frac{\partial ds}{\partial t}, \quad (9)$$

where Λ is the mobility of filaments and \vec{J} is the total current of integrin molecules on the membrane, which includes the following terms:

$$J_{attraction} = \frac{\kappa \Lambda \bar{H}}{n_s} n \nabla H, \quad (10)$$

$$J_{dispersion} = -\frac{\kappa \Lambda \bar{H}^{-2}}{n_s} n \nabla n, \quad (11)$$

$$J_{interaction} = \Lambda c \Omega n \nabla n, \quad (12)$$

$$J_{diffusion} = -D \nabla n, \quad (13)$$

where $J_{attraction}$ is the attractive flux resulting from interaction between the integrin molecules through the membrane curvature, $J_{dispersion}$ is the dispersive flux due to the membrane resistance to integrin aggregation resulting from their membrane bending effects, $J_{interaction}$ is the flux due to the direct interaction between integrin molecules, and $J_{diffusion}$ is the usual thermal diffusion flux, which depends on the diffusion coefficient, $D = \Lambda kT$. The last term in Eq. (9) arises from the covariant derivative of the density with time on a contour, whose length evolves with time. In this term ds is the infinitesimal contour (line) element. This term ensures that the total number of integrin molecules is conserved as the contour length changes. Note that the fluxes due to entropy were not taken into account due to their relatively small magnitude.

In present study the results were calculated using numerical simulations of the dynamics of the model system beyond the linear limit. The above explained differential equations were solved using an explicit Euler method in Matlab. We checked for the convergence of our one-dimensional simulations, in space and time. A variation of the Monge representation $h(s)$ was employed to simplify the numerical computation, such that the curvature force was kept only up to linear order. For simplicity, the boundary conditions on the nearly flat membrane were taken to be periodic. The following is a list of the parameter values incorporated in our numerical simulations: $\varphi_s = 0.008 \text{ g}\mu\text{m}^{-2}$, s^{-2} , $\kappa = 100 \text{ kT}$, $\bar{H} = 10 \text{ }\mu\text{m}^{-1}$, $\sigma_f = 0.001 \text{ g s}^{-2}$, $\omega = 1.10^{-3} \text{ g}\mu\text{m}^2\text{s}^{-2}$, $c = 4$, $\Omega = 3.5 \cdot 10^{-6} \text{ g}\mu\text{m}^2\text{s}^{-2}$, $n_s = 100 \mu\text{m}^{-2}$, $\xi = 125 \text{ s}^{-1}\text{g}$, $D = 0.002 \text{ }\mu\text{m}^2\text{s}^{-1}$.

RESULTS OF NUMERICAL SIMULATIONS

Previously, it has been shown experimentally that nanotube surfaces facilitate the binding of osteoblast cells only when the nanotube diameter was 15-20 nm. On the other hand, osteoblasts on large diameter nanotube surfaces (>30 nm) formed fewer focal contacts, while demonstrating

more cell death. In the present model, the binding and interaction of integrin molecules were incorporated into the free energy equation using a negative binding energy term and a negative interaction term (Eq.(1)). The underlying assumption of our model was that the binding and interaction constants were positive only in the osteoblast membrane regions directly above the nanotube surface (edge) regions.

We then performed a linear stability analysis in the approximation of a nearly flat membrane shape. The dynamics in our system was driven by two mechanisms. The instability that leads to the initial growth of membrane protrusions was driven by the interplay between the positive membrane surface tension, negative binding potential, and direct interaction energy. The instability in the system was stabilized by membrane embedded integrin molecules that flowed into favourably curved membrane regions, thereby reducing the free energy of the system. The above dynamics was driven by a positive feedback loop in which the influx of integrin molecules towards favourable curvature regions increased the positive membrane curvature, leading to further attraction of integrin molecules. In the numerical simulations presented (Fig. 3), it was assumed that the osteoblast membrane at the start was positioned 10 nm above the flat nanotube surface, where the total length of the membrane was $2\mu\text{m}$ (Fig. 3). Furthermore, a random perturbation of small amplitude <1% of the integrin density was added around the initial uniform density of the integrin molecules.

The conditions for instability were satisfied only for the small diameter nanotube surface, at which initial membrane growth was observed (Fig. 3). During the simulation, larger membrane protrusions were formed by the coalescence of smaller membrane protrusions. The large membrane protrusions eventually adhered to the titanium surface, trapping the adhering membrane regions by the end of the simulation (Fig. 3). In contrast, no growth was observed for the large diameter nanotube surface (Fig. 3).

CONCLUSIONS

In the present study, a dynamic model was employed to demonstrate that in the limit of a large binding potential for integrin molecules at the edges of vertically oriented TiO_2 nanotubes, there is a strong attraction of the cell membrane to the small diameter nanotube surface. The small diameter nanotube surface has a significantly larger portion of strong integrin binding regions (*due to the larger area density of highly curved nanotube edges*) than the large diameter nanotube surface. In addition, the extracellular part of the integrin molecules (of conical shapes) can easily bind to neighboring nanotubes on the small diameter nanotube surface, since the interacting integrin molecules are in contact with the nanotube edges. Certainly this is not possible on a nanotube surface having too large hollow interior space.

Here, it was proposed that the observed aggregation of integrin molecules forming focal adhesion is additionally enhanced on small diameter nanotubes because the extracellular part of integrin molecules is of similar size, enabling crossbinding over the edges of neighboring nanotubes. We suggest that the enhanced growth of the cell membrane on a

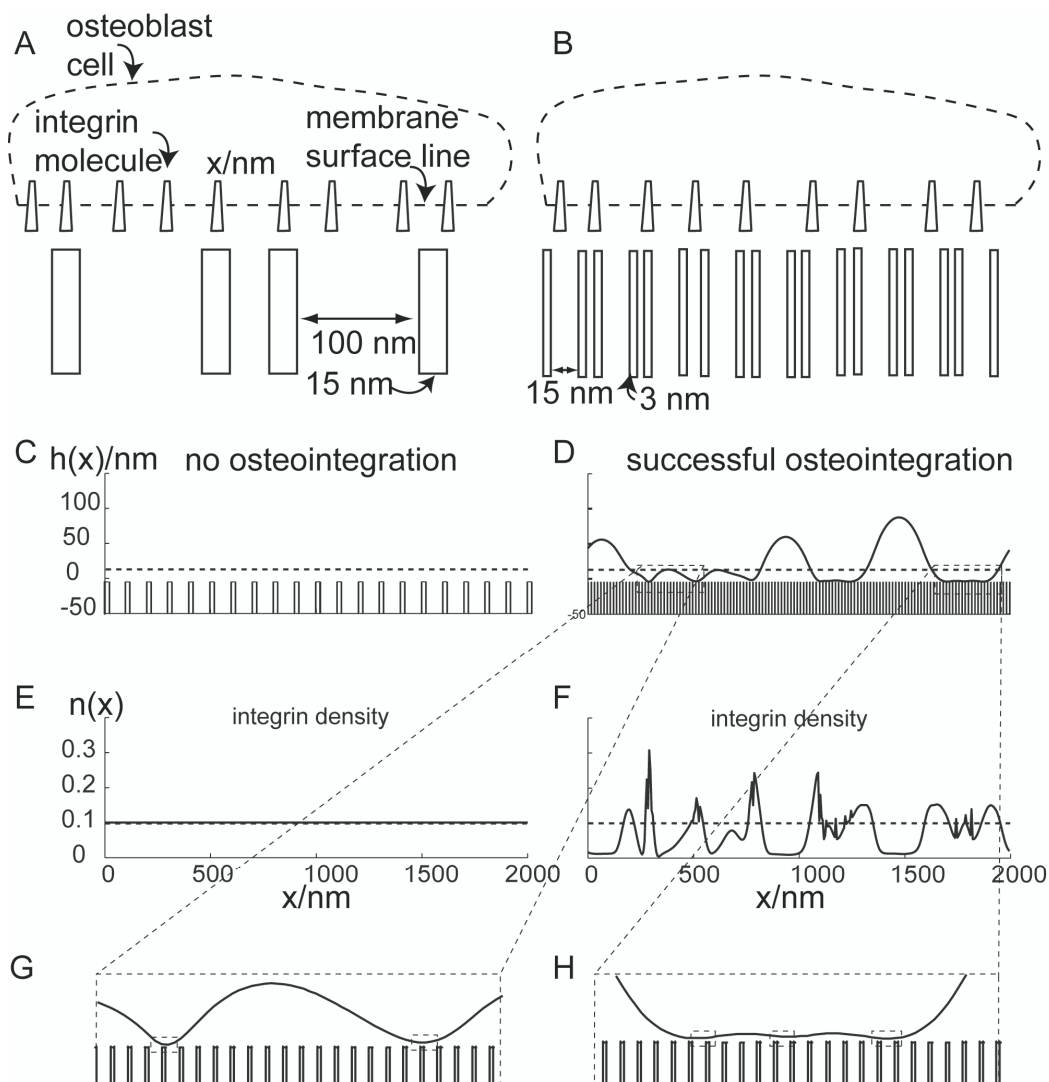


Fig. (3). The effects of large and small diameter nanotube surfaces on the theoretically predicted membrane shape and adhesion. The modelled membrane segment with a distribution of integrin molecules of positive spontaneous curvature is positioned 10 nm above the large diameter (100 nm) surface (A) or above the small diameter (15 nm) nanotube surface (B). The vertical cross-section of the nanotube is modelled explicitly as a rectangular edge-like profile. The binding and interaction energies facilitated by the nanotube surface are incorporated into the free energy by having non-zero integrin binding and interaction potentials above the nanotube edge regions, while above the void regions (i.e. across the nanotube diameter) the binding and interaction potentials are zero. Steady state membrane shapes ($h(x)$) and integrin density distributions ($n(x)$) for the adhesion of an osteoblast membrane to the large diameter (100 nm) (C,E) and the small diameter (15 nm) (D,F) nanotube surfaces are plotted. Close-up views of membrane growth on the 15 nanotube surface demonstrates the uneven adhesion of cell membrane to the nanotube surface (G,H).

vertically oriented nanotube surface is facilitated by the interaction of integrin molecules during the formation of a focal adhesion.

The TiO₂ nanotube surface has an increased surface charge density at the sharp edges which promotes the adsorption of fibronectin and vitronectin molecules, and proteins with a quadrupolar internal charge distribution. The result is a more efficient adhesion and spread of osteoblasts to the vertically oriented TiO₂ nanotubes (Fig. 2). The fact that the small diameter nanotube surface has on average more sharp edges per unit area with an increased surface charge density in comparison to the large diameter nanotube

surface (Fig. 1) may explain why the osteoblast binding affinity of a small diameter nanotube surface is larger than the binding affinity of one of large diameter. Based on the experimental results presented in this work (Fig. 2) and the recent suggested mechanism of protein-mediated attractive interaction between a negatively charged surface and negatively charged osteoblasts [5, 6] (as well as to cation mediated binding of fibronectin [17] and electrostatic binding of vitronectins), we suggest that the negative surface charge density at highly curved edges of a TiO₂ nanotube wall surface contributes to the increased strength of osteoblast adhesion.

CONFLICT OF INTEREST

The authors confirm that this article content has no conflicts of interest.

ACKNOWLEDGEMENTS

This work was supported by Slovenian Research Agency grants J3-2120, J1-4109, J1-4136, J3-4108 and P2-0232. The authors are grateful for help to N. Gov and M. Pazoki for useful discussions. The first two authors E.G. and D.K. share the first authorship equally.

DISCLOSURE

Parts of the information included in this review article have previously been published in *Int. J. Nanomed.*, **2011**, *6*, 1801-1816 (ref. [6]).

REFERENCES

- [1] Anselme, K. Osteoblast adhesion on biomaterials. *Biomaterials*, **2000**, *21*, 667-681.
- [2] Boby, J.D.; Wilson, G.J.; MacGregor, D.C.; Pilliar, R.M.; Weatherly, G.C. Effect of pore size on the peel strength of attachment of fibrous tissue to porous-surfaced implants. *J. Biomed. Mater. Res.*, **1982**, *16*, 571-584.
- [3] Papat, K.C.; Chatvanichkul, K.I.; Barnes, G.L.; Latempa T.J.; Grimes, C.A.; Desai, T.A. Differentiation of marrow stromal cells cultured on nanoporous alumina surfaces. *J. Biomed. Mater. Res. A.*, **2007**, *80*, 955-964.
- [4] Puckett, S.; Pareta, R.; Webster, T.J. Nano rough micron patterned titanium for directing osteoblast morphology and adhesion. *Int. J. Nanomedicine*, **2008**, *3*, 229-241.
- [5] Kabaso, D.; Gongadze, E.; Perutkova, Š.; Kralj-Iglič, V.; Matschegewski, C.; Beck, U.; van Rienen, U.; Iglič, A. Mechanics and electrostatics of the interactions between osteoblasts and titanium surface. *Comput. Meth. Biomech. Biomed. Eng.*, **2011**, *14*, 469-482.
- [6] Gongadze, E.; Kabaso, D.; Bauer, S.; Slivnik, T.; Schmuki, P.; van Rienen, U.; Iglič, A. Adhesion of osteoblasts to a nanorough titanium implant surface. *Int. J. Nanomed.*, **2011**, *6*, 1801-1816.
- [7] Park, J.; Bauer, S.; von der Mark, K.; Schmuki, P. Nanosize and vitality: TiO₂ nanotube diameter directs cell fate. *Nano Lett.*, **2007**, *7*, 1686-1691.
- [8] Ilie, I.; Ilie, R.; Mocan, T.; Bartos, D.; Mocan, L. Influence of nanomaterials on stem cell differentiation: designing an appropriate nanobiointerface. *Int. J. Nanomedicine*, **2012**, *7*, 2211-2225.
- [9] Park, J.; Bauer, S.; Schmuki, P. von der Mark K. Narrow window in nanoscale dependent activation of endothelial cell growth and differentiation on TiO₂ nanotube surfaces. *Nano Lett.*, **2009**, *9*, 3157-3164.
- [10] Walboomers, F.F.; Jansen, J.A.; Jansen, J.A. Cell and tissue behavior on micro-grooved surface. *Odontology*, **2001**, *89*, 2-11.
- [11] Monsees, T. K.; Barth, K.; Tippelt, S.; Heidel, K.; Gorbunov, A.; Pompe, W.; Funk, R. H. W. Surface patterning on adhesion, differentiation, and orientation of osteoblast-like cells. *Cell. Tiss. Org.*, **2005**, *180*, 81-95.
- [12] Smeets, R.; Kolk, A.; Gerressen, M.; Driemel, O.; Maciejewski, O.; Hermanns-Sachweh, B.; Riediger, D.; Stein, J.M. A new biphasic osteoinductive calcium composite material with a negative zeta potential for bone augmentation. *Head Face Med.*, **2009**, doi: 10.1186/1746-160X-5-13.
- [13] Smith, I. O.; Baumann, M. J.; McCabe, L.R. Electrostatic interactions as a predictor for osteoblast attachment to biomaterials. *J. Biomed. Mater. Res. A.*, **2004**, *70*, 436-441.
- [14] Urbanija, J.; Bohinc, K.; Bellen, A.; Maset, S.; Iglič, A.; Kralj-Iglič, V.; Sunil Kumar, P.B.S. Attraction between negatively charged surfaces mediated by spherical counterions with quadrupolar charge distribution. *J. Chem. Phys.*, **2008**, *129*, 105101.
- [15] Urbanija, J.; Tomšič, N.; Lokar, M.; Ambrožič, A.; Čučnik, S.; Rozman, B.; Kandušer, M.; Iglič, A.; Kralj-Iglič, V. Coalescence of phospholipid membranes as a possible origin of anticoagulant effect of serum proteins. *Chem. Phys. Lipids*, **2007**, *150*, 49-57.
- [16] Zelko, J.; Iglič, A.; Kralj-Iglič, V.; Kumar, P.B.S. Effects of counterion size on the attraction between similarly charged surfaces. *J. Chem. Phys.*, **2010**, *133*, 204901.
- [17] Heath, M. D.; Henderson, B.; Perkin, S. Ion-specific effects on the interaction between fibronectin and negatively charged mica surfaces. *Langmuir*, **2010**, *26*, 5304-5308.
- [18] Rapuano, B. E.; MacDonald, D.E. Surface oxide net charge of a titanium alloy: modulation of fibronectin-activated attachment and spreading of osteogenic cells. *Coll. Surf. B*, **2011**, *82*, 95-103.
- [19] Stevens, M.; George, J.H. Exploring and engineering the cell surface interface. *Science*, **2005**, *310*, 1135-1138.
- [20] Schar, C.R.; Blouse, G.E.; Minor, K.H.; Peterson, C.B. A deletion mutant of vitronectin lacking the Somatomedin B domain exhibits residual plasminogen activator inhibitor-1-binding activity. *J. Biol. Chem.*, **2008**, *283*, 10297-10309.
- [21] Xu, D.; Baburaj, K.; Peterson, C.B.; Xu, Y. Model for the three-dimensional structure of vitronectin: predictions for the multi-domain protein from threading and docking. *Proteins*, **2001**, *44*, 312-320.
- [22] Frank, M.; Sodin-Šemrl, S.; Rozman, B.; Potočnik, M.; Kralj-Iglič, V. Effects of low-molecular-weight heparin on adhesion and vesiculation of phospholipid membranes a possible mechanism for the treatment of hypercoagulability in antiphospholipid syndrome. *Ann. N. Y. Acad. Sci.*, **2009**, *1173*, 874-886.
- [23] Butt, H.J.; Graf, K.; Kappl, M. *Physics and Chemistry of Interfaces*, Wiley-VCH, Weinheim, **2003**.
- [24] Memming, R. *Semiconductor electrochemistry*, Wiley-VCH Verlag GmbH, **2001**.
- [25] Veksler, A.; Gov, N. Phase transitions of the coupled membranecytoskeleton modify cellular shape. *Biophys. J.*, **2007**, *93*, 3798-3810.
- [26] Kabaso, D.; Shlomovitz, R.; Auth, T.; Lew, L. V.; Gov, N. Curling and local shape changes of red blood cell membranes driven by cytoskeletal reorganization. *Biophys. J.*, **2010**, *99*, 808-816.
- [27] Kabaso, D.; Lokar, M.; Kralj-Iglič, V.; Veranič, P.; Iglič, A. Temperature and cholera toxin B are factors that influence formation of membrane nanotubes in RT4 and T24 urothelial cancer cell lines. *Int. J. Nanomedicine.*, **2011**, *6*, 495-509.
- [28] Kabaso, D.; Shlomovitz, R.; Schloen, K.; Stradal, T.; Gov, N.S. Theoretical model for cellular shape transitions driven by protrusive and adhesive forces. *PLoS Comp. Biol.*, **2011**, *7*, 1-13.
- [29] Kralj-Iglič, V. Stability of membranous nanostructures: a possible key mechanism in cancer progression. *Int. J. Nanomedicine*, **2012**, *7*, 3579-3596.
- [30] Kralj-Iglič, V.; Heinrich, V.; Svetina, S.; Žekš, B. Free energy of closed membrane with anisotropic inclusions, *Eur. Phys. J. B.*, **1999**, *10*, 5-8.